Photoelectron and Photofragment Velocity Imaging Following the Excitation of CH_3I to the A-Band Using fs, ps, and ns Laser Pulses

Peter C. Samartzis,[†] Bernard L. G. Bakker,[‡] David H. Parker,[‡] and Theofanis N. Kitsopoulos*,[†]

Department of Chemistry, University of Crete and Institute of Electronic Structure and Laser, Foundation for Research and Technology-Hellas, 711 10 Heraklion-Crete, Greece, and Department of Molecular and Laser Physics, University of Nijmegen, Toernooiveld, 6525 ED Nijmegen, The Netherlands

Received: March 3, 1999; In Final Form: May 18, 1999

Multiphoton processes following the excitation of methyl iodide to the A-band continuum are studied using a pulsed laser beam of 5 eV photons with pulse duration of 15 ns, 5 ps, and 500 fs. Velocity map images are obtained for the resulting photoelectron, I^+, and CH_3^+ fragments. Both one-photon dissociation and multistep ionization are observed, the latter process becoming dominant at the shorter pulse duration. The photoelectron spectra (PES) obtained from velocity map imaging, which provides uniform transmittance for all electron kinetic energies, show that two-photon excitation of CH_3I mediated by the dissociative A-band leads to the production of excited CH_3I^+ ions with non-Franck−Condon intensity distributions. The vibrational distributions obtained are compared with zero kinetic energy (ZEKE) and magnetic bottle PES measurements under similar conditions. Velocity images of the I^+ and CH_3^+ show a marked anisotropy whose angular dependence on the scattering angle varies strongly with the laser pulse duration. At progressively shorter pulse durations, multiphoton ionization/fragmentation of CH_3I^+ dominates the observed signal.

Introduction

Photoexcitation of methyl iodide to the A-band (first dissociation continuum) produces methyl radicals plus ground-state and spin-orbit excited iodine atom fragments, which we label hereafter as $I(^2P_{3/2})$ and $I^*(^2P_{1/2})$, respectively. Three dissociative excited electronic states, designated as $^3Q_0$, $^3Q_1$, and $^1Q_1$ by Mulliken,[1−3] are optically accessible from the ground state. The $^3Q_0$ state correlates asymptotically to CH_3+I^*, while excitations to the $^3Q_1$, and $^1Q_1$ states lead to the production of CH_3+I. Despite numerous studies of this photodissociation process, which have been summarized in several articles,[4−6] deconvolution of the contributions of each of these states to the overall A-band cross-section remained experimentally unresolved. Recently, the partial absorption cross-sections have been determined[7] for each state using the technique of velocity mapping,[8] demonstrating also in this way the method's capability to successfully address difficult questions in chemical dynamics. Contrary to previous studies,[9] the $^1Q_1$ state is found to contribute less than 1% to the total A-band absorption spectrum.

Because of its relatively strong absorption cross-section, the dissociative A-band region of CH_3I provides a path for exciting higher lying electronic states or probing the structure of CH_3I^+ by photoionization, an experimental approach pioneered by Colson and co-workers.[10] For methyl iodide, such intermediate-enhanced two-step photoionization experiments have been reported using both zero kinetic energy (ZEKE)[11−13] and conventional photoelectron spectroscopy (PES).[14] Two independent ZEKE experiments were performed using ns laser systems, while the PES experiment used a 2.5 ps laser system operating at 252.5 or 251 nm. Each of the above-mentioned studies reported that all six normal modes of the CH_3I^+ ion are excited during the photoionization. These findings deviate from the predictions based on the Franck−Condon factors (FCF) calculated between the ground-state ion and the neutral molecule, which indicate that only transitions with $\Delta v = 0$ should have appreciable intensity. This behavior was attributed to the dissociative A-band intermediate, whereby the CH_3I begins to stretch its C−I bond length during the dissociation process, just prior to absorbance of the second photon that excites the molecule to the ionization continuum. The change in C−I bond length modifies the FCF sufficiently such that the overtone transitions gain considerable intensity.

Theoretical treatment of the two-photon ionization of CH_3I through the A-band has been performed by Abrashkevich and Shapiro,[15] referred to hereafter as AS. Their analysis, in sharp contrast to the experimental observations, predicts mostly excitation of the combination bands of the ν_3 and ν_2 (CH_3 umbrella bend) modes. Initially this discrepancy was attributed to possible artifacts in peak intensities of ZEKE spectra. However, in light of the conventional PES spectra of Schultz and Fischer,[14] referred to hereafter as SF, whose intensities agree with the those of the ZEKE data, this possibility should be discounted. SF suggested that a possible explanation could be inaccuracies in the potential energy surfaces for the intermediate states. Other indications of inaccuracies in the potential energy surfaces were found in a study of the internal energy distributions of the CH_3 fragments using velocity mapping.[16] SF also point out that the shape of the PES spectrum changes drastically with small changes in the dissociation laser wavelength, which implies that very subtle changes in the intermediate geometry impact the appearance of the PES spectrum tremendously. To verify this statement, in this report we present the two-photon photoelectron spectrum of CH_3I at 248 nm measured via

* E-mail: theo@luce.iesl.forth.gr.
[†] University of Crete and Institute of Electronic Structure and Laser.
[‡] University of Nijmegen.

10.1021/jp990750z CCC: $18.00
Published on Web 07/20/1999

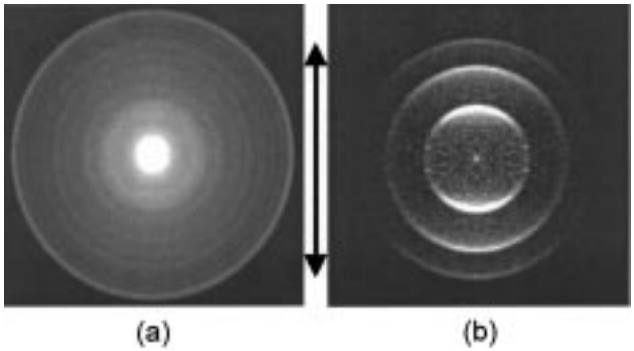

Figure 1. (a) Two-photon photoelectron image of CH_3I at 248.6 nm using a 5 ps pulse duration. (b) Two-photon photoelectron image of NO at 248.6 nm using a 5 ps pulse duration. The arrow indicates the laser polarization direction. Lighter areas in these grayscale images refer to higher signal levels.

photoelectron velocity mapping. In addition, we also record the velocity distribution of the I^+ and CH_3^+ product, which yields extra information concerning the competition between ionization and dissociation of the A-band.

Experimental

The experimental apparatus used in this study has been described in detail elsewhere.[17,18] Briefly, a cold molecular beam is produced by expanding a gas mixture (typically 5% CH_3I in He) into the source chamber via a home-built pulsed nozzle (backing pressures $P_0 \leq 1$ atm). The molecular beam, which is skimmed and collimated to ~0.8 mm diameter, is intersected at right angles by a laser beam generated by a KrF excimer pumped-dye laser system capable of producing 15 ns, 5 ps, and 500 fs laser pulses.[19] This is a one-color experiment so the same laser is used for both for the A-band excitation of CH_3I and subsequent *non-resonant* ionization of either the parent molecule or the neutral photofragments (e.g., I, I*, or CH_3). The laser light is vertically polarized (parallel to the plane of the two-dimensional detector) and is focused using a lens with a 20 cm focal length. The laser beam is attenuated to the point where no more than ~100 ions/shot are created, in order to avoid space charge problems. Typically, 500 μJ pulses are used. Ions or electrons produced in the interaction region are accelerated by a suitable electric field[8,18] along the axis of the time-of-flight mass analyzer and are detected using a home-built position-sensitive ion-imaging detector.[17] Discrimination against background cations is achieved by gating the detector, so results presented in this article are obtained by recording the CH_3^+ and $^{127}I^+$ ion signal. Details about the image processing techniques and extraction of velocity distributions can be found in ref 17. In the case of photoelectron imaging, no detector gating is necessary, while magnetic shielding made up of two sections of concentric tubes (Ø140−Ø150 mm and Ø70−Ø80 mm) rolled from a 0.5 mm thickness μ-metal sheet are installed along the axis of the spectrometer to screen the electrons from the earth's magnetic field.

Results

Typical velocity map images for photoelectrons produced from the two-photon ionization of methyl iodide using a 5 ps laser pulse are presented in Figure 1(a). Images obtained using a 500 fs pulse are very similar to the 5 ps pulse, while the photoelectron image using a nanosecond pulsed laser was too weak to analyze. The 5 ps and 500 fs photoelectron images consist of a very intense center part, and a series of isotropic concentric rings, the brightest of which appears on the outer edge. Calibration of the CH_3I photoelectron images is performed using the NO photoelectron image shown in Figure 1(b), produced from the two-photon ionization of NO (ionization potential 9.26 eV) under identical conditions to that of Figure 1(a). The spectrum shows a series of three anisotropic rings, with most of the intensity appearing along the laser polarization direction.

Typical velocity map images for I^+ and CH_3^+ produced from the irradiation of methyl iodide at 248 nm are presented in Figures 2 and 3, respectively. The velocity distribution of the I^+ product (and CH_3^+) appears to depend strongly on the laser pulse duration. Specifically, we note that as the pulse duration shortens, the images tend to become more anisotropic with an increased amount of intensity along the laser polarization direction and a narrowing of the image "waist" along the equator. In addition, the partially resolved ring structure of the ns duration image shown in Figure 2(a) is absent in both the ps and fs duration images shown in Figures 2(b) and 2(c), respectively. In the CH_3^+ image shown in Figure 3, a set of two weak discs can be seen more clearly at higher velocities, above which are superimposed a much stronger anisotropic and continuous kinetic energy structure as seen in the I^+ images. The two weak discs arise from the nonresonant ionization[17] of the methyl fragments formed in the I and I* channels after one-photon dissociation of the parent molecule.

The photoelectron and I^+ speed or kinetic energy distributions, which we determine by appropriate reconstruction of either the e^- or I^+ images[17,20] are shown in Figures 4, 5, and 6, respectively. The I^+ kinetic energy distribution has been divided up into three regions labeled as inner, middle, and outer. The relative intensity of these regions changes with laser pulse duration such that the inner region appears nearly invariant, while the middle and outer regions are essentially identical for both the ps and fs durations but differ substantially from the ns results.

Discussion

A. Photoelectron Spectra. In the case of the two-photon ionization of NO, the photoelectron speed distribution consists of three peaks which correspond to formation of $NO^+(v = 0, 1, 2)$ from the processes

$$NO + 2h\nu\ (248\ nm) \rightarrow NO^+\ [(v = 0, 1, 2), J] + e^- \quad (1)$$

Our experimental resolution is limited by the size of a single ion spot on our detector, typically 2−3 pixels wide (~200 μm). This spot size is common to all parts of the detector, a statement confirmed by our ability to model the NO photoelectron speed distribution using three Gaussian functions of identical widths (Figure 4(a)). The area of each peak corresponds to the Franck−Condon factor for this transition, and, since the simulation peak widths are the same, the area of each peak is proportional to its height. The calculated positions and Franck−Condon factors[21] using Morse potentials for NO and NO^+ and a temperature of 50 K are overlaid in the same plot, and clearly the agreement to our experimental values is excellent. This justifies the use of photoelectron velocity mapping as a suitable technique for quantitative measurements of the photoelectron spectra. It is noteworthy that the corresponding kinetic energy of the slowest peak is only 135 meV, and yet it is detected with the same efficiency and signal-to-noise ratio as the higher energy peaks. This efficiency of detecting slow e^- results from the acceleration of the nascent photoelectrons to energies of ≥750 eV, thus

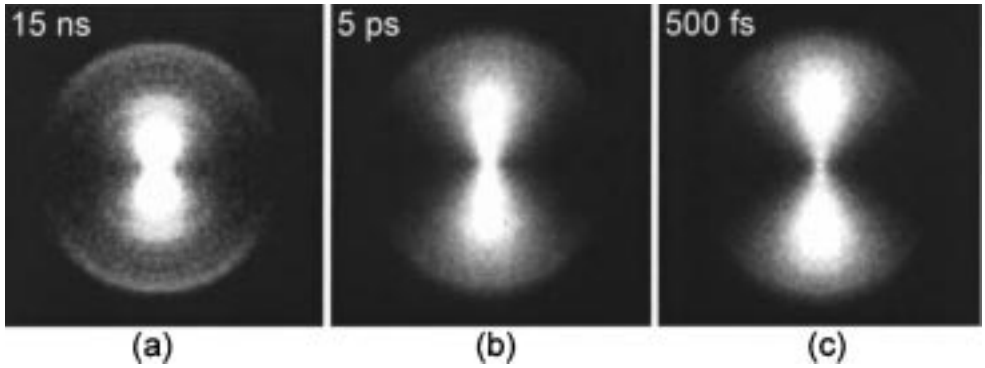

Figure 2. I^+ photofragment images following the photolysis of CH_3I at 248.6 nm using: (a) 15 ns pulse duration, (b) 5 ps pulse duration, and (c) 500 fs pulse duration.

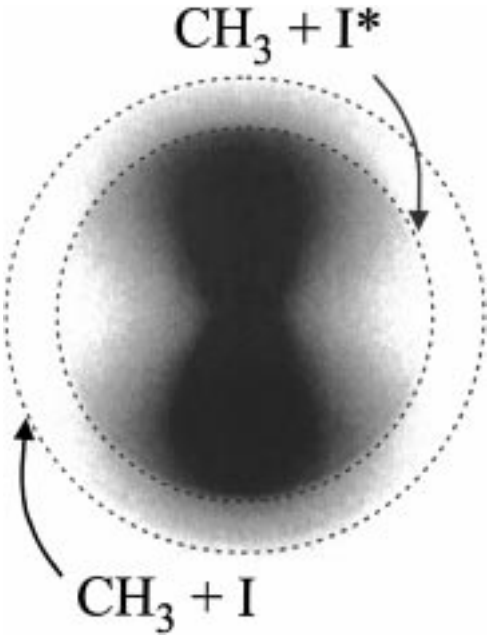

Figure 3. CH_3^+ photofragment image following the photolysis of CH_3I at 248.6 nm using a 5 ps pulse duration. In order to enhance the weaker signals, the image is presented as inverted grayscale where the (off-scale) darker areas refer to higher signal levels. The maximal kinetic energy releases (minimal CH_3^+ internal energy) are indicated by dashed circles for the I and I* channels.

minimizing the effects of stray fields. The resolution ($\Delta E/E$) at the outermost ring, NO^+ ($v = 0$), is ~6%. In principle, one could image photoelectrons just above threshold (true ZEKEs) with 1 meV of energy, in which case the energy resolving power of the velocity imaging technique would be ~0.06 meV (0.5 cm^{-1}), a resolution comparable to the bandwidth of conventional ns laser systems.

The photoelectron speed distribution of CH_3I shown in Figure 4(b) consists of a dominant peak assigned to the origin band, followed by a series of fairly regularly spaced peaks. As in both the ZEKE[12,13] and the PES[14] experiment, we initially assign the structure in the spectrum to a pure ν_3 overtone progression. We therefore model our spectrum using a series of fixed-width Gaussian functions similar to those used in the NO calibration spectrum. This single mode fit, along with the expected positions for a progression in the C−I stretch is shown in Figure 4(b). The fit is poor, especially when compared to the calibration fit of NO photoelectron spectrum (Figure 4(a)). As both the NO and CH_3I spectra are obtained under identical experimental conditions, one doesn't expect any degradation of the experimental resolution between the two systems. Here it is assumed that essentially all of the photoelectrons arise from CH_3I ionization. Furthermore, the intrinsic width of the CH_3I PES peaks is (like NO) assumed to be less than the apparatus function, which is determined by the size of a single ion event. Consequently, we are led to believe that the assumption of a single ν_3 overtone progression is not sufficient to explain our measured CH_3I photoelectron spectrum.

Naturally, adding more Gaussian functions improves the fit to the experimental data, yielding the results shown in Figure 4(c). This is a best-fit population spectrum using all possible CH_3I^+ vibrations and their combinations, following the approach of SF. The estimated uncertainty is at least 2% in total population for the stronger vibrations ($\geq$ 10% of the total $v > 0$ population) and higher fractional uncertainty for the weaker peaks. The positions and heights of the underlying stick spectra represent the position and intensity of each Gaussian function used in the fit. Also shown above the spectrum are the positions for vibrations corresponding to the six normal modes of CH_3I^+ and the ν_2 ($v = 1$), ν_3 combination band. The agreement between the predicted positions and the results of the fit is very satisfying, and the spectral assignments are listed in Table 1. We are unable to distinguish the overtone transition 3_0^3 from the 5_0^1 and the transition 6_0^2 from the $2_0^1 3_0^1$ because of their close proximity in the spectrum, and consequently we only report their cumulative contribution to the overall spectral intensity.

In Figure 5 we plot the populations of each vibrational progression separately and compare our results with the ZEKE experiments and the theoretical predictions. We note that only modes ν_2, ν_3, and the combination mode $\nu_2\nu_3$ were considered in the calculations of AS. Our intensities have been scaled such that the $\nu_3(\Delta v = 4)$ intensity in the ZEKE spectrum of SF agrees with ours. Although quantitatively there is disagreement between our data and the theoretical predictions, there are interesting qualitative similarities. Specifically, we observe that in both cases the ν_3 vibrational progression shows several local maxima, which in our data occur at $\Delta v = 1$ (overall maximum), 4, and 7, while for the theory they correspond to $\Delta v = 1$, 5, and 9 (not shown). This trend is not observed in the ZEKE spectra where the ν_3 progression shows a single peak at $\Delta v = 4$. Also, the intensities of the combination bands $\nu_2\nu_3$ decrease almost linearly beyond the $2_0^1 3_0^2$ transition in both the calculations of AS and our experiment, while this trend is reversed in the ZEKE experiment. In the ZEKE experiments the dominant feature in the spectrum is the $\Delta v = 4$ transition, while in the SF photoelectron spectra (shown in Figure 6(a), our work, and the theoretical calculations, the origin band is the strongest feature. SF attributed this difference in the relative strengths of the overtone and origin band amongst the ZEKE (ns experiments) and PES (ps experiments) to what they called *simultaneous*

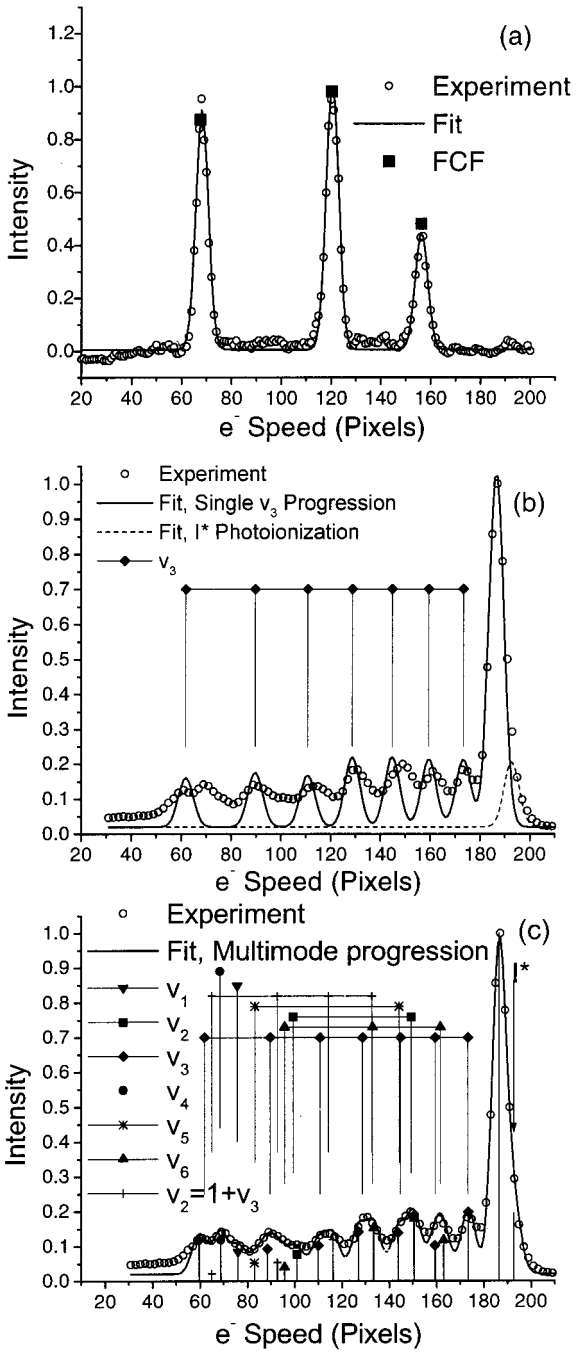

Figure 4. (a) Photoelectron speed distribution produced from the photoionization of NO at 248.6 nm (5 ps). (b) Experimental and single-mode simulation of the photoelectron speed distribution produced from the photoionization of CH_3I at 248.6 nm (5 ps). (c) Experimental and multimode mode simulation of the photoelectron speed distribution produced from the photoionization of CH_3I at 248.6 nm (5 ps). A series of 20 Gaussian functions, whose positions and intensities are listed in Table 1, is used to fit the spectrum.

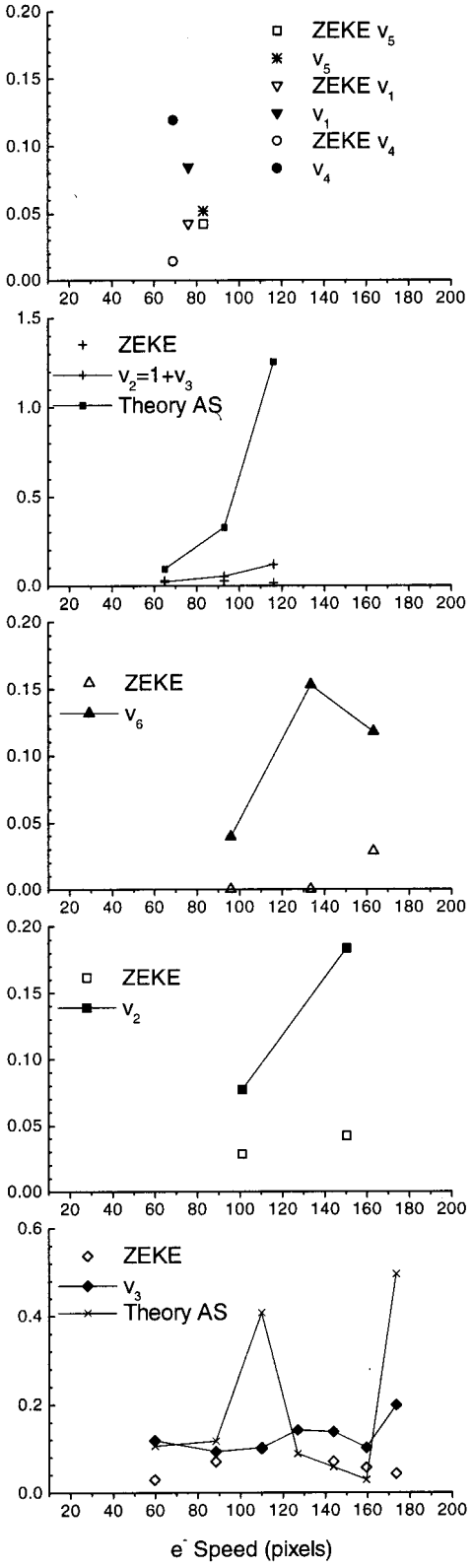

Figure 5. Comparison of our overtone spectral intensities with those of the ZEKE experiment from ref 13 and theoretical calculation from ref 15.

rather than *sequential* two-photon absorption. In other words, because of the facile ionization achieved using short pulse length lasers, the direct simultaneous process will contribute intensity only to the origin band because it is this transition that has the dominate FCF between the ground states of the ion and the neutral. This effect, however, should not change the relative intensities of the spectral features within the overtone progression. If this were the case, then using an even more intense laser field (shorter pulse duration), the relative intensity of the origin band should become even greater than in the case of the ps PES spectra. Inspection of Figure 6(a) where both ps and fs photoelectron kinetic energy spectra are shown, indicates that no such effect occurs and that the 500 fs and 5 ps PES spectra are nearly identical. The slight broadening of the peaks in the 500 fs spectrum is caused by the increased bandwidth of the shorter pulse duration. Hence we believe that the explanation

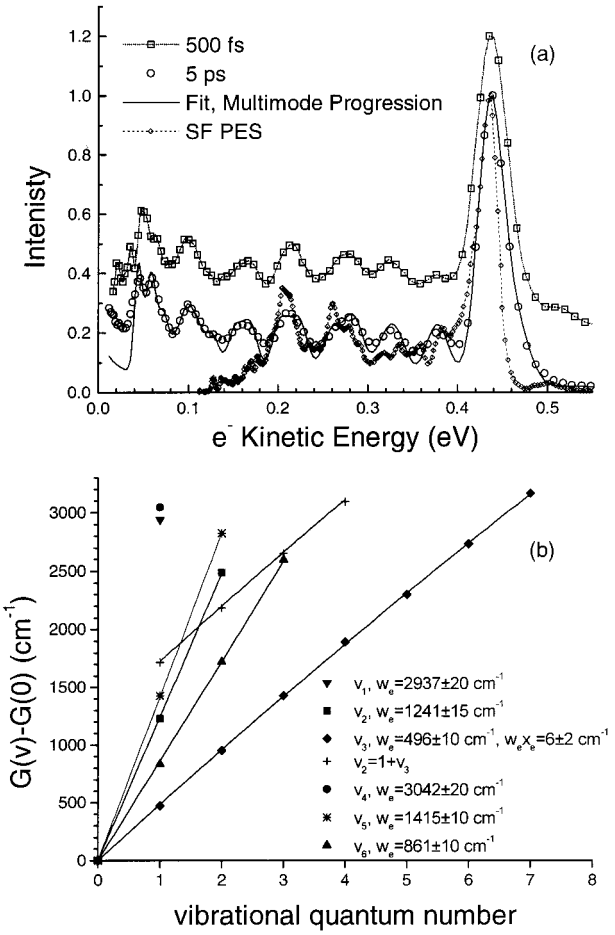

Figure 6. (a) Experimental and simulated photoelectron kinetic energy distribution produced from the photoionization of CH_3I at 248.6 nm. Also shown are the results of SF ref 14. (b) Vibrational energy spacings for the observed progressions in the photoelectron spectra.

TABLE 1: Intensities, Positions, and Spectral Assignments of the Gaussian Functions Used to Simulate the Spectrum Shown in Figure 4(c)

position (pixels)	position (eV)	intensity (±10%)	assignment
192.7	0.466	1.40	$I^* \rightarrow I^+ + e^-$
186.5	0.437	7.14	0_0^0
173.5	0.378	1.42	3_0^1
163.0	0.333	0.84	6_0^1
159.4	0.319	0.73	3_0^2 and 5_0^1
150.5	0.284	1.31	2_0^1
143.8	0.259	0.99	3_0^3
133.5	0.224	1.09	2_0^1, 3_0^1, and 6_0^2
127.0	0.202	1.01	3_0^4
115.0	0.166	0.85	2_0^1, 3_0^2
110.0	0.152	0.73	3_0^5
101.0	0.128	0.55	2_0^2
95.7	0.115	0.28	6_0^3
92.8	0.108	0.38	2_0^1, 3_0^3
88.5	0.098	0.66	3_0^6
83.0	0.086	0.37	5_0^2
76.0	0.072	0.6	1_0^1
68.8	0.059	0.85	4_0^1
65.0	0.053	0.15	2_0^1, 3_0^3
59.6	0.045	0.84	3_0^7

proposed by SF appears to be insufficient in settling the discrepancy between the ZEKE and PES experiments.

Summing up the total intensity in each overtone progression ($v > 0$), we conclude that the highest propensity belongs to the ν_3 mode (47%) followed by ν_6 (16%), ν_2 (14%), $\nu_2\nu_3$ (10%), ν_4 (6%), ν_1 (4%), and ν_5 (3%). These are relative fractions of the $v > 0$ peaks, which themselves comprise ~66% of the total PES. Not only are there long progressions in ν_3, also each possible vibrational mode in CH_3I^+ has some population. As this non-Franck−Condon behavior arises from the influence of the A-band intermediate state, the observed CH_3I^+ vibrational distribution can be compared with the internal energy partitioning observed in methyl iodide photofragmentation via the A-band. Removal of an I atom from CH_3I results in the cancellation of two vibrational modes, ν_3(a), and also the doubly degenerate ν_6(e), corresponding to the off-axis methyl rocking motion. The other four modes of CH_3I, ν_1(a), the C−H stretch, ν_2(a) umbrella mode, ν_4(e) asymmetric C−H stretch, and ν_5(e) methyl rocking deformation correspond to the ν_1(a), ν_2(a), ν_3(e), and ν_4(e) modes in CH_3, respectively, with roughly the same internal coordinates.

The dominance of the ν_3 mode in CH_3I^+ is expected as this is the dissociation coordinate of CH_3I upon excitation to the A-band. Studies of the CH_3 product state distributions find that methyl radical produced in conjunction with ground-state I atoms have substantial amounts of excitation in the ν_2 umbrella mode. In contrast, the CH_3 radical produced by the I* channel is quite cold. The yield of I atoms at 248 nm is ~20%, with ~30% of the methyl fragments in this channel in $v = 0$. The remaining ν_2 population in $v > 0$ is thus 14% in agreement with the 14% propensity we find for the ν_2 mode in CH_3I^+.

The other dissociation coordinate, ν_6, is also found to be populated in CH_3I^+. When the neutral molecule is thermally populated in this mode, the excess vibrational energy is found to convert almost completely to translational energy in the fragments.[16] It is believed that coupling between the dominant optically active state $^3Q_0$ (A_1 symmetry, correlates to I*) and the higher lying $^1Q_1$ state (E symmetry, correlates to I) is caused by Jahn−Teller distortion (e⊗E) of the C_{3v} symmetry of $^1Q_1$ state via this ν_6 (e-symmetry) rocking vibration. This curve crossing process results in the production of I atoms with a 20% yield as mentioned above. Once again, this I/I* yield is comparable to the 16% propensity found in this study for the ν_6 mode in CH_3I^+. Concerning the $\nu_2\nu_3$ combination mode, as a first approximation, one can assume that its propensity should be equal to the product of the individual mode propensities, i.e., 47%*14% = 7%, close to the 10% value determined from our spectra simulations.

The total ν_1 (C−H stretch) activity in CH_3 from the photolysis of CH_3I at 248 nm has been reported[16] to be ~8%, with most of the activity in the I atom channel. In ref 16, and previous TOF measurements, it is difficult to quantitatively separate the methyl C−H stretch motions ν_1 and ν_3, while ν_3 activity is not observable in the CH_3 IR emission and REMPI measurements reported previously. It appears from our measurements that ν_3 in CH_3 (equivalent to the observed ν_4 mode in CH_3I^+) is active, but to a lesser extent than ν_1. Finally, a small amount (3%) of ν_5 activity is indicated in CH_3I^+. This motion corresponds to ν_4 in CH_3, and interestingly, evidence for a small amount of ν_4 motion in CH_3 has recently been reported.[16]

In general, it appears that the vibrational excitation patterns observed here in CH_3I^+ compare very favorably with those observed for CH_3 radicals produced at the same dissociation wavelength. While the present observations are not quantitative, they do suggest that the two very different measurements − intermediate state influenced CH_3I^+ photoelectron spectroscopy and photofragment end-product analysis − yield essentially the same results. It could be expected that the PES measurements

TABLE 2: Estimated Frequencies for the Six Normal Modes of CH_3I^+ Observed in the Photoelectron Spectrum

mode	ν_1	ν_2	ν_3	ν_4	ν_5	ν_6
ω_e (cm^{-1})	2937 ± 20	1241 ± 15	496 ± 10	3042 ± 20	1415 ± 10	861 ± 10
$\omega_e x_e$ (cm^{-1})			6 ± 2			

would probe much earlier time scales in the photodissociation process than the asymptotic end product measurements. That both measurements yield similar results may suggest that the vibrational propensities are mainly determined at the absorption step of the process rather than by the topological details of the potential energy surfaces reached later in the photodissociation event. This could also partially explain the wavelength dependence of the CH_3I^+ PES reported by SF, who reported drastic changes in the appearance of their PES upon changing excitation wavelengths between 252.5 and 251 nm, the main difference being the relative importance of the 3_0^1 overtone in the spectrum. However, in the intermediate state influenced PES spectra, an extra wavelength dependence in the second absorption step ($A \rightarrow X(^2\Pi_{3/2})$ CH_3I^+) may arise because of autoionization of Rydberg states converging to the higher $^2\Pi_{1/2}$ spin-orbit component. It should be noted that the vibrational yield patterns in CH_3 radicals were found in ref 16 to be relatively invariant to changes in the dissociation wavelength. In any case, the consistency of the overtone propensities determined from velocity mapping with those determined from photodissociation studies is thus quite encouraging and lends support to the proposed spectral assignments given in Figure 4.

The photoelectron kinetic energy distributions obtained from the speed distributions are shown in Figure 6(a). From the assignments in Table 1 and using the relationship

$$G(v) - G(v=0) = (\omega_e - \omega_e x_e)v - \omega_e x_e v^2 \qquad (2)$$

ω_e and $\omega_e x_e$ are obtained by plotting $G(v) - G(v=0)$ vs v, as shown in Figure 6(b). The results listed both in Figure 5(b) and in Table 2 are in very good agreement with previous spectroscopic measurements.[13] If we compare our results to PES of SF at 252.5 nm (Figure 6(a)), they appear to be consistent up to 0.2 eV. Although our total two-photon energy is only 99 meV (802 cm^{-1}) higher then the excitation energy used by SF, we observe a far greater number of ν_3 overtones. Specifically, while SF were unable to reliably measure photoelectrons beyond the $v = 4$ overtone, we observe 7 quanta of excitation in the C−I stretch, thus reaching the energetic limit defined by our total photon energy. This discrepancy could be attributed to either an experimental shortcoming in the SF study or extremely sensitive dynamics of the A-band. Concerning the former experimental explanation, the inherent transmission limitations of the magnetic bottle analyzer used by SF could prohibit the observation of overtones up to their energetic limit of $v = 6$. The great advantage of the imaging method is that it not only offers *4π collection efficiency* but, in addition, it has uniform transmittance for all particle velocities. Furthermore, because velocity mapping is a distance-of-flight method, no Jacobian correction factors are needed as in the more common time-of-flight experiments.

B. Photofragment Kinetic Energy Distributions. *B.1. Iodine Atom Images.* The kinetic energy distribution (KED) for the I^+ photofragment is shown in Figure 7. As mentioned earlier, it is known that upon excitation of methyl iodide to the A-band at 248 nm the molecule dissociates, producing both I and I* with a branching ratio I/(I+I*) ≈ 20%. Hence one possible mechanism for I^+ formation is nonresonant ionization of these neutral iodine photofragments. The energy of a single photon in our current experiment is 4.987 eV, which means that three photons

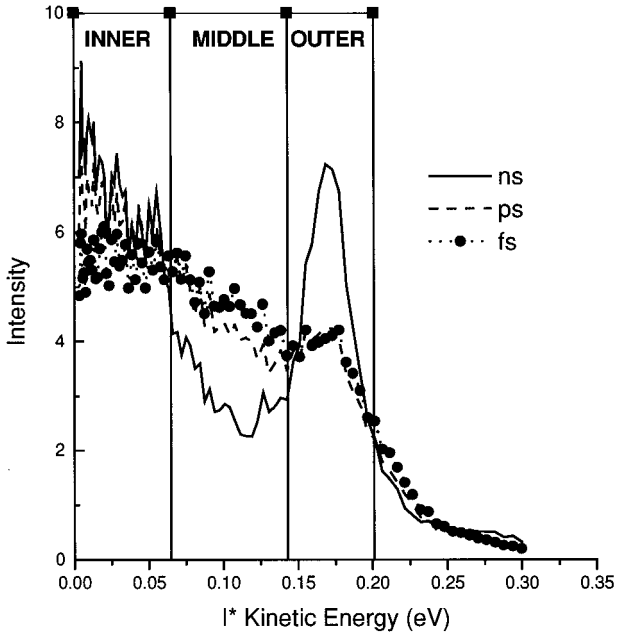

Figure 7. Photofragment I^+ kinetic energy distributions.

are necessary to ionize ground-state iodine (I.P. = 10.454 eV) and two photons to (auto)ionize I* (I.P. = 9.511 eV).

Evidence for I atom ionization can be verified by the presence of a corresponding peak in the photoelectron kinetic energy spectrum. The kinetic energy of the electrons produced from three-photon ionization of I atoms would be 4.5 eV, *too large* to be detected under our current experimental capabilities. Given our limiting acceleration voltage (5 kV) and the length of our TOF spectrometer (45 cm), photoelectrons with greater than ~3 eV of energy in the center-of-mass frame (such as those produced from three-photon ionization of I), fly off our detector. However, photoionization of nascent I* atoms does appear to occur, as is suggested in the photoelectron spectrum in Figure 4(b), where a partially resolved shoulder at the highest kinetic energy is assigned to this process. This peak in the PES could also be due in part to CH_3I hot band activity ($\Delta v = -1$), however, which was found to be active under similar conditions in ref 16. The intensity of the I* ionization peak when compared to the rest of the 5 ps PES spectrum is relatively small in any case. An observation of I* atom ionization is less surprising than I atom ionization as the overall mechanism of this process involves three photons, one photon needed for the dissociative excitation to the A-band and two for the ionization, whilst the photoionization of CH_3I is a two-photon process.

With regard to the I^+ signal, CH_3 photofragments produced in conjunction with I* atoms have been found to be internally cold,[22] and consequently a narrow KED for the I* photofragments in the I^+ spectrum is expected. From Figure 7 we see that the I^+ KED is bimodal, and the position of the peak at the highest kinetic energy is consistent with formation and ionization of I* atoms. As a second confirmation a tunable dye laser operating at similar conditions to the 248 nm nanosecond laser was used to photodissociate and resonantly ionize I atoms at 247.9 nm. In this case, the dominant peak in the image appears at the kinetic energy expected for one-photon dissociation of CH_3I into CH_3 plus I* atoms. *Nonresonant* ionization using the

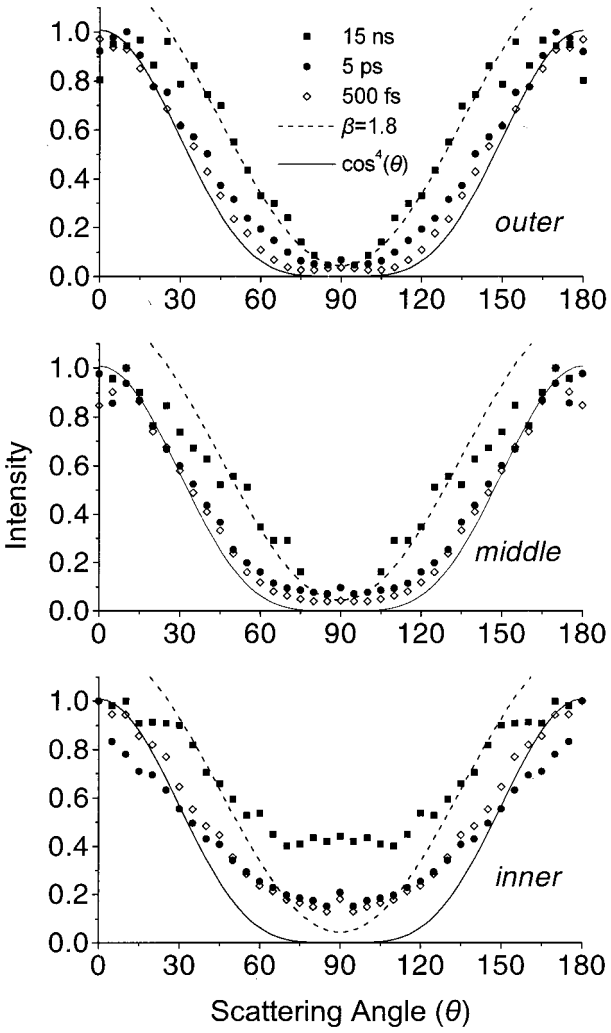

Figure 8. Photofragment I^+ angular distributions for the kinetic energy regions indicated in Figure 7.

KrF laser system at 248 nm thus produces I^+ via two mechanisms, the higher energy peak being due to ionization of I* atoms formed from one-photon dissociation of CH_3I.

An alternative method of producing I^+ is the postionization photodissociation of CH_3I^+, which means that the daughter CH_3I^+ ions absorb another photon, are excited to a dissociative continuum, and then decompose into I^+ and CH_3 (or $I+CH_3^+$). Using the known values of the ionization potentials for I (10.454 eV), CH_3I (9.54 eV), and the dissociation energy of CH_3I (2.42 eV), the energy needed to dissociate CH_3I^+ into $I^+(^3P_2)$ and CH_3 is ~3.33 eV. Should all of the excess energy be channeled into translation, this would produce an I^+ peak at nearly the same position as the I* atom peak from neutral CH_3I dissociation. While most of the previous studies of the photodissociation of CH_3I^+ have been performed at lower excitation energies,[23,24] Szaflarski and El-Sayed[25] have reported the kinetic energy distributions of I^+ and CH_3^+ fragments following the ionization of CH_3I using a 30 ps laser operating at 266 nm. They found an average kinetic energy release for I^+ of 0.05 ± 0.03 eV, which compares favorably with the KED of the slower component seen in Figure 7(a). Calculations using a statistical model for the fragment kinetic energy based on the Franklin approximate formula[25] agreed well with the experimental observations at 266 nm. In contrast to the present work at 248 nm, direct two-photon ionization of CH_3I is not possible at 266 nm. Our photoelectron spectrum shows that the dominant channel at 248 nm is the formation of CH_3I^+, which is then dissociated with a third 5.0 eV photon. Because the CH_3I^+ is formed in a wide range of vibrational modes, a wider distribution of I^+ kinetic energies may also be expected. When increasing the laser intensity by way of decreasing the pulse duration, we notice that the relative amount of the fast vs the slow peak in the I^+ KED decreases. This would imply that under these conditions, namely stronger (more intense) laser fields, the propensity for ionization of the A-band is greater than that for dissociation.

B.2. Methyl Radical Image. Figure 3 is an image of CH_3^+ obtained using a 5 ps laser at 248 nm. While the methyl radical does not absorb in the near UV region, with sufficient laser intensity it is possible to ionize the molecule via two-photon, nonresonant, three-photon ionization, as has been observed previously in studies of CH_3Br[17] and CH_3I.[16] The two weak discs seen in Figure 3 at higher velocities arise from this nonresonant ionization of the methyl fragments formed in the I *and* I* atom channels after one-photon dissociation of the parent molecule. The corresponding signal for this process should appear around 0.14 eV in the photoelectron spectrum. There is no significant peak seen at this energy, confirming that nonresonant photoionization of CH_3 radicals is a very minor channel compared to production of CH_3^+ from CH_3I^+. In the velocity map images of CH_3^+ using 500 fs pulses (not shown), the anisotropic middle part of the image, from CH_3I^+ photodissociation, completely dominates the higher velocity CH_3 two-photon ionization signal.

C. Photofragment Angular Distributions. The ground-state symmetry of CH_3I is A_1 while the symmetry of the three excited states forming the A-band is E for the $^3Q_1$, $^1Q_1$ states and A_1 for the $^3Q_0$ state. Assuming a prompt dissociation and an axial recoil of the photofragments, then the excitation to the $^3Q_0$ state will be a parallel transition, namely producing angular distributions $I(\theta) \propto \cos^2\theta$,[26,27] and since I* correlates to the $^3Q_0$ state, i.e., anisotropy parameter, $(I^*) = 2.0$. Deviations from this ideal value are caused by the nonadiabatic coupling between the $^3Q_0$ and $^1Q_1$ and have been observed and quantified.[7] For an excitation wavelength of 248 nm, the measured anisotropy parameter for I* is $(I^*) \approx 1.8$. Given our assignments for the features in the I^+ KED, by integrating the *outer* region we should obtain an angular distribution characteristic for I*. For the ns pulse duration, our experimental results shown in Figure 7(a) are in good agreement with the value $(I^*) = 1.8$. For the ps and fs pulse durations, however, the I^+ angular distributions resemble a $\cos^4(\theta)$ functional form. This is a reassuring result, given our earlier conclusion that at shorter laser pulse durations, fragmentation of the CH_3I^+ rather than ionization of I* produced from the A-band dissociation is the primary source of I^+.

A question remains in explaining the observed $\cos^4(\theta)$ angular distribution for the CH_3I^+ photodissociation. For a one-photon dissociation process, as we mentioned above, the extreme functional forms for the photofragment angular distributions are $\cos^2(\theta)$ and $\sin^2(\theta)$. When angular distributions with higher order terms in $\cos(\theta)$ are observed, this usually signifies either a multiphoton process or an alignment effect.[26,28,29,30] The $\cos^4(\theta)$ dependence is expected in a two-photon excitation where parallel transitions are involved in both steps. In our experiment, the photoionization step involves two photons, and therefore such a process could generate aligned daughter ions with the desired $\cos^4(\theta)$ angular distribution. However, the proposed alignment could eventually wash out on a time scale similar to that of a rotational period, which for CH_3I^+ is ~1 ps.

An alternative alignment explanation is related to the interaction of the strong electric fields produced by short pulse lasers with atoms and molecules. Estimations of the laser field intensities at the interaction volume under our experimental conditions are approximately 10^6 to 10^7 W/cm^2 (ns duration), 10^{11} to 10^{12} W/cm^2 (ps duration), and 10^{12} to 10^{13} W/cm^2 (fs duration). The laser field intensities for the ps and fs situations are high enough that they could cause an alignment of the CH_3I parent molecules prior to their dissociative photoionization.[31−33] The strong laser field induces a dipole moment which then tends to *trap* the molecule in pendular states, causing them to librate about the electric field direction (laser polarization direction). The magnitude of this effect increases with increasing field strength and polarizability of the molecule.[31] This behavior is entirely consistent with our experimental observations, and we believe it is the mechanism causing the $\cos^4(\theta)$ angular distribution.

Conclusions

Methyl iodide is excited to the A-band continuum using 5 eV laser photons with pulse durations of 15 ns, 5 ps, and 500 fs. Both ionization and dissociation of A-band are observed, the former process becoming dominant at the shorter pulse durations. The photoelectron spectrum is dominated by two-photon, nonresonant ionization of CH_3I and consists of non-Franck−Condon overtone progressions in a surprisingly large number of modes. Velocity images of I^+ and CH_3^+ show two channels, a dominant channel with a broad energy distribution due to dissociation of CH_3I^+, which becomes increasingly anisotropic at shorter pulse durations, and a much weaker signal due to nonresonant, two-photon ionization of the neutral fragments created at the one-photon level. At shorter pulse lengths ionization appears to compete effectively with dissociation at the one-photon level.

Acknowledgment. We acknowledge Apostolis Egglezis for maintaining the KrF fs-ps-ns laser system up and running. This work is conducted at the Ultraviolet Laser Facility operating at FORTH-IESL (TMR, Access to Large Scale Facilities EU program, Contract No. CHGE-CT92-007) and is also supported by TMR Network *IMAGINE* ERB 4061 PL 97-0264.

References and Notes

(1) Mulliken, R. S. *J. Chem. Phys.* **1940**, *8*, 382.
(2) Mulliken, R. S. *Phys. Rev.* **1942**, *61*, 277.
(3) Mulliken, R. S.; Teller, E. *Phys. Rev.* **1942**, *61*, 283.
(4) Johnson, B. R.; Kittrell, C.; Kelly, P. B.; Kinsey, J. L. *J. Phys. Chem.* **1996**, *100*, 7743.
(5) Amamatsu, Y.; Yabushita, S.; Morokuma, K. *J. Chem. Phys.* **1996**, *104*, 9784 and references therein.
(6) Amamatsu, Y.; Morokuma, K.; Yabushita, S. *J. Chem. Phys.* **1991**, *94*, 4894 and references therein.
(7) Eppink, A. T. J. B.; Parker, D. H. *J. Chem. Phys.* **1998**, *109*, 4758.
(8) Eppink, A. T. J. B.; Parker, D. H. *Rev. Sci. Instrum.* **1997**, *68*, 3477.
(9) Gedanken, A.; Rowe, M. D. *Chem. Phys. Lett.* **1975**, *34*, 39.
(10) Li, L.; Lipert, R. J.; Park, H.; Chupka, W. A.; Colson, S. D. *J. Chem. Phys.* **1987**, *87*, 6767.
(11) Zhu, Y. F.; Grant, E. R. *J. Phys. Chem.* **1993**, *97*, 9582.
(12) Strobel, A.; Lochschmidt, A.; Fischer, I.; Niedner-Schatteburg, G.; Bondybey, V. E. *J. Chem. Phys.* **1993**, *99*, 733.
(13) Strobel, A.; Fischer, I.; Lochschmidt, A.; Müller-Dethlefs, K.; Bondybey, V. E. *J. Phys. Chem.* **1994**, *98*, 2024.
(14) Schultz, T.; Fischer, I. *J. Phys. Chem. A* **1997**, *101*, 5031.
(15) Abrashkevich, D. G.; Shapiro, M. *J. Chem. Phys.* **1996**, *105*, 9493.
(16) Eppink, A. T. J. B.; Parker, D. H. *J. Chem. Phys.* **1998**, *109*, 4758; **1999**, *110*, 832.
(17) Samartzis, P. C.; Sakellariou, I.; Gougousi, T.; Kitsopoulos, T. N. *J. Chem. Phys.* **1997**, *107*, 43.
(18) Gougousi, T.; Samartzis, P. C.; Kitsopoulos, T. N. *J. Chem. Phys.* **1998**, *108*, 5742.
(19) Schäfer, F. P.; Szatmári, S. *Optics Comm.* **1988**, *68*, 196.
(20) Chandler, D. W.; Kitsopoulos, T. N.; Buntine, M. A.; Baldwin, D. P.; McKay, R. I.; Heck, A. J. R.; Zare, R. N. *Gas-Phase Chemical Reaction Systems: Experiments and Models 100 Years after Max Bodenstein*; Wolfrum, J., Volpp, H.-R., Rannacher, R., Warnatz, J., Eds.; Springer Series in Chemical Physics (Springer Berlin: Heidelberg, 1996).
(21) Arnold, D. W., Ph.D. Thesis, University of California at Berkeley, 1994, and references therein.
(22) Chandler, D. W.; Janssen, M. H. M.; Stolte, S.; Strickland, R. N.; Thoman, J. W., Jr.; Parker, D. H. *J. Phys. Chem.* **1990**, *94*, 4839.
(23) Walter, K.; Weinkauf, R.; Boesl, U.; Schlag, E. W. *J. Chem. Phys.* **1988**, *89*, 1914.
(24) Syage, J. A.; Steadman, J. *Int. J. Mas Spectrom. Ion Proc.* **1996**, *159*, 125.
(25) Szaflarski, D. M.; El-Sayed, M. A. *J. Phys. Chem.* **1988**, *92*, 2234.
(26) Zare, R. N. *Mol. Photochem.* **1972**, *4*, 1.
(27) Yang, S.; Bersohn, R. *J. Chem. Phys.* **1974**, *61*, 4400.
(28) Sander, R. K.; Wilson, K. R. *J. Chem. Phys.* **1975**, *63*, 4242.
(29) Kawasaki, M.; Sato, H.; Kobayashi, A.; Arikawa, T. *Chem. Phys. Lett.* **1988**, *146*, 101.
(30) Sander, R. K.; Wilson, K. R. *J. Chem. Phys.* **1975**, *63*, 4242.
(31) Friedrich, B.; Herschbach, D. *Phys. Rev. Lett.* **1995**, *74*, 4623.
(32) Normand, D.; Lompre, L. A.; Cornaggia, C. *J. Phys. B.* **1992**, *25*, L497.
(33) Ravindra Kumar, G.; Cross, P.; Stefvan, C. P.; Rajgara, F. A.; Mathur, D. *Phys. Rev. A* **1996**, *53*, 3098.